Program Digest, 2019 IEEE International Ultrasonics Symposium (IUS)
Glasgow, Scotland, October 6-9, 2019

Experimental validation of a novel technique for ultrasound imaging of cardiac fiber orientation

Alessandro Ramalli
Dept. of Cardiovascular Sciences
KU Leuven
Leuven, Belgium
ORCID: 0000-0003-4358-3739

Emeline Turquin
Univ Lyon, INSA-Lyon, Université Claude Bernard Lyon 1, UJM-Saint Etienne, CNRS, Inserm, CREATIS UMR 5220, U1206
Lyon, France

Lorena Petrusca
Univ Lyon, INSA-Lyon, Université Claude Bernard Lyon 1, UJM-Saint Etienne, CNRS, Inserm, CREATIS UMR 5220, U1206
Lyon, France

François Varray
Univ Lyon, INSA - Lyon, Université Claude Bernard Lyon 1, UJM-Saint Etienne, CNRS, Inserm, CREATIS UMR 5220, U1206
Lyon, France

Jan D'hooge
Dept. of Cardiovascular Sciences
KU Leuven
Leuven, Belgium

***Abstract*— The arrangement of cardiac fibers determines mechanical and electrical properties of the heart and can be altered due to pathology. Hence, the non-invasive assessment of fiber characteristics is of interest from both a pathophysiologic and a diagnostic point of view. Recently, we proposed and validated, by computer simulations, a theoretical framework to have more insight on 3D ultrasound Backscatter Tensor Imaging. The theory showed that spatial coherence (SC) maps of echo signals, across the probe aperture, not only carry information on fiber direction, but also on fiber size and pitch. The aim of this study was to experimentally validate these findings and conduct preliminary *in vivo* tests. Experiments were conducted on a purposely designed and built phantom consisting of several sets of parallel nylon wires, having different diameter (S) and pitch (P). Finally, preliminary tests were conducted on the biceps of healthy volunteers. Experiments confirmed the simulation results: averaged over all acquisitions, the main-to-secondary lobe distance linearly correlated with P (R^2=94%), while the value of the SC at lag 1 (an estimate of the main lobe width) linearly correlated with S (R^2=48.6%). *In vivo* results demonstrated the feasibility of extracting microstructural information of the tissue by the analysis of SC maps.**

Keywords*— *Fiber orientation, Cardiac imaging, Plane waves, Spatial coherence.

I. Introduction

Major cardiovascular diseases, the leading cause of death in the Western developed countries [1], [2], are often associated with a reduced ability of the left ventricle to pump blood to the body. Often, it is linked to a disorder of the myoarchitecture [3]–[5], i.e. the complex 3D network of muscle fibers [6]–[9], which governs the mechanical and electrical properties of the heart, determining its function [10]–[12]. Hence, the assessment of fiber characteristics is of primary interest from both a pathophysiologic and a diagnostic point of view.

This work was supported by the European Union's Horizon 2020 research and innovation programme under the Marie Skłodowska-Curie grant agreement No 786027 (ACOUSTIC project) and by Internal Funds University of Leuven grant (PF/10/014).

Cardiologists have been aware, for at least a century, of the evidence that fiber orientation varies across the myocardial walls [13], [14] and, nowadays, most of the medical imaging modalities have their own technique for the estimation of cardiac fiber orientation: magnetic resonance imaging [15], [16], x-ray [17], [18], optical tomography [19], [20], microscopy [21], [22], and ultrasound [23]–[25]. The latter, in particular, has the particularity of being non-invasive and having good temporal resolution. However, even if the 3D ultrasound Backscatter Tensor Imaging (3D-BTI), the state-of-the-art, showed promising results of the orientation of the cardiac fiber during the cardiac cycle [25], it is unclear which histologic structure it detects. Therefore, to address this issue, we recently proposed and validated, by computer simulations, a different theoretical framework [26]. It showed that spatial coherence (SC) maps of echo signals, across the probe aperture, not only carry information on fiber direction, but also on fiber size (S) and pitch (P). Specifically, the main-to-secondary lobe distance of SC was shown to relate to P, while the width of its main lobe to S. On the other hand, however, the minimum detectable P is equal to twice the pitch among the elements of the probe, thus setting a lower limit to the detectable distance between fibers. Therefore, the aim of this study was to experimentally validate these findings and conduct preliminary *in vivo* tests.

II. Method

A. Theoretical background basics

In [26], we related the autocorrelation of the backscattered signals to the spatial coherence (SC) of a tissue under exam, when transmitting a single plane wave with a 2D matrix of transducers. The theory showed that, for an unfocused transducer, the spatial coherence of the backpropagated field on the probe plane ($R_{E_B}(x,y,0)$) equals the autocorrelation ($R\{\cdot\}$) of the spatial scattering amplitude distribution ($\eta(x,y,z_F)$) of the area illuminated by the transmitted beam ($E_I(x,y,z_F)$):

$$R_{E_B}(x,y,0) = R\{E_I(x,y,z_F)\cdot\eta(x,y,z_F)\} \quad (1)$$

where z_F is the depth of the plane where the fibers are located. Moreover, for a plane wave transmitted by a square aperture of side A,

$$E_I(x, y, z_F) = \Pi\left(\frac{x}{A}\right) \cdot \Pi\left(\frac{y}{A}\right) \quad (2)$$

where $\Pi(\cdot)$ is the rectangular function, defined as:

$$\Pi(\cdot) = \begin{cases} 1, & if\ |\cdot| < 1/2 \\ 0, & if\ |\cdot| \geq 1/2 \end{cases} \quad (3)$$

B. Experiments

1) Homemade phantom

A homemade phantom was purposely designed and built, it included several sets of 80-mm long mounted on a plexiglass frame as shown in the schematic sketch of Fig. 1. Each set consisted of several parallel wires, having different diameter (S=128, 200, 400 µm) and pitch (P=800, 1200, 1600 µm) and it was approximately 14 mm wide. The frame was mounted on a homemade rotating plate that allowed full 360°-rotation in steps of 2.5°. Also, the frame could be moved so that the rotation axis was matched to the middle point of each set of wires. Doing so, different orientations of the wires with respect to the probe could be tested.

2) Experimental setup

The operations of four Vantage 256 scanners (Verasonics, Kirkland, USA) were synchronized to realize a 1024-channel system [27]. Each channel was individually connected to an element of a 2D matrix array (Vermon S.A., Tours, France). It consists of 32 (x-axis) by 35 (y-axis) elements (3.0 MHz, 300 µm pitch, 70% bandwidth), but on the y-direction every ninth row is not connected. Hence, the total number of addressable elements is 1024. All elements of the probe were excited simultaneously with a 1-cycle square burst, at a central frequency of 3 MHz and with a peak amplitude of 30V, to transmit a not steered plane wave. Radiofrequency echo signals were acquired and post-processed.

The wire phantom was placed at a distance of 20 mm from the probe surface. Different acquisitions were conducted, by matching the rotation axis of each set of wires, red-crosses in Fig. 1, to the propagation axis of the plane wave. Then, 4 orientation angles were considered (0°, 30°, 60°, 90°), where 0° means that the wires were parallel to the x-axis.

Finally, preliminary tests were conducted on the biceps of healthy volunteers. Data sets were collected for different positions of the probe with respect to the long axis of the biceps.

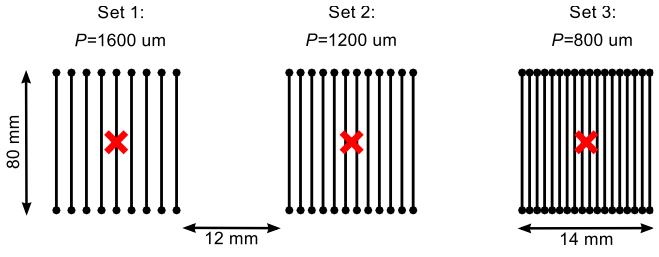

Fig. 1 Schematic top-view of the homemade phantom. Horizontal and vertical scale are differrent. The red crosses correspond to the middle point of each set. A similar setup was built for wires with different diameters (S=128, 200, 400 µm).

C. Post-processing

As detailed in [26], the wire/fiber orientation was estimated as the angle corresponding to the maximum of the Radon transform of the 2D spatial coherence function, which was computed as:

$$R(\Delta x, \Delta y) = \frac{1}{(N_x - |\Delta x|) \cdot (N_y - |\Delta y|)} \cdot \quad (4)$$

$$\cdot \sum_{x_i} \sum_{y_i} \frac{\sum_{t=T_1}^{T_2} S_{RF}(x_i, y_i, t) \cdot S_{RF}(x_i - \Delta x, y_i - \Delta y, t)}{\sqrt{\sum_{t=T_1}^{T_2} S_{RF}(x_i, y_i, t)^2 \cdot S_{RF}(x_i - \Delta x, y_i - \Delta y, t)^2}}$$

Where $S_{RF}(x_i, y_i, t)$ is the radiofrequency echo signal received on the i-th element with coordinates x_i, y_i, while T_1 and T_2 are the two ends of the averaging temporal window. It is worth highlighting that, according to the proposed theory, $S_{RF}(x_i, y_i, t)$ is the signal as it is received, without applying any dynamic focusing delay.

III. Results & Discussion

Examples of the 2D spatial coherence maps, computed according to (4), are shown in the left panels of Fig. 2. It these acquisitions, obtained on phantom, the orientation of the wires was 30°, the diameter was S=200 µm, while the pitch was P=800 (top) and 1200 µm (bottom). As expected from the theory, the maps present a main lobe having its main direction along Δy', the orientation of which resulted 30° and 29° for P=800 and 1200 µm, respectively. Also, the maps qualitatively show that the main-to-secondary lobe distance increases for higher P values. This is better highlighted in the right panel of Fig. 2, it shows the SC profiles obtained along Δx', i.e. along the direction orthogonal to Δy'. Specifically, it highlights how the position of the secondary lobe peaks matches quite well the theoretical expected position (dotted lines). Moreover, it also highlights that the width of the main lobes at Δx'=1 closely fits

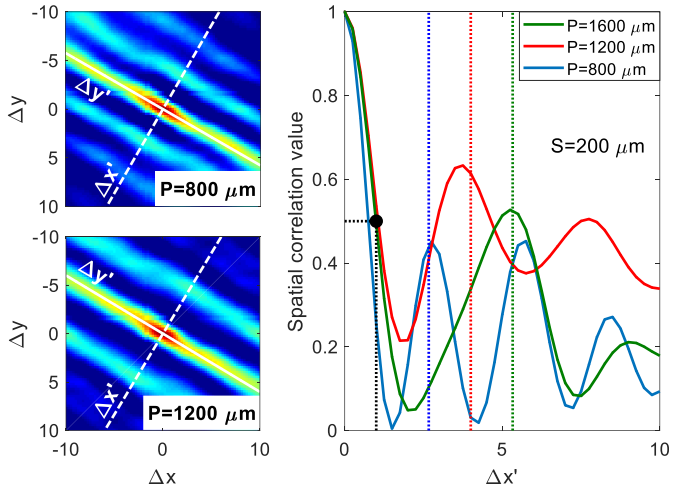

Fig. 2 Left panels: examples of SC maps obtained for S=200 µm and P=800 (top) and 1200 µm (bottom). Right panel: SC profiles obtained along Δx' axis obtained for different S=200 µm and different P values. The colored dotted lines highlight the expected positions of side-lobes peak, while the black dot poitns to the expected width of the main lobe.

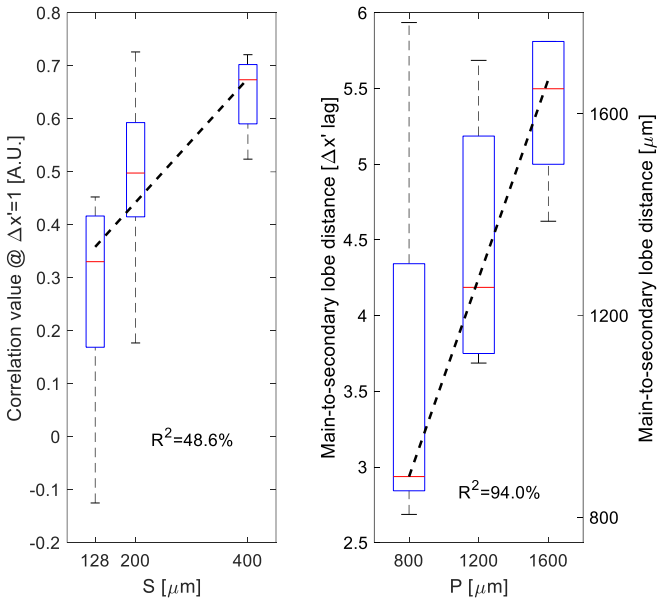

Fig. 3 Left: distribution of the correlation value computed at lag Δx'=1 for different fiber sizes S. Right: distribution of the main-to-secondary lobe distance for different fiber pitches P. The black dashed lines represent the linear fitting of the two distributions.

to the expected value (black dot).

Similar results were obtained also for S=128 and 400 µm and for the 4 different orientations (0°, 30°, 60°, 90°) of the wires as summarized in Fig. 3. Averaged over all acquisitions, the value of the SC at lag 1 (Fig. 3 left), considered as an estimate of the main lobe width, linearly correlated with S (R^2=48.6%). Furthermore, Fig. 3 right shows that the main-to-secondary lobe distance linearly correlated with P (R^2=94%). Specifically, in agreement with the theoretical background, on average, the main-to-secondary lobe distance is equal to P.

Finally, Fig. 4 shows examples of SC maps obtained *in vivo* on the bicep of a healthy volunteer at two different positions. Qualitatively, the maps are similar to those obtained on phantom, i.e. they present a main lobe and parallel secondary lobes. According to the findings shown in Fig. 3, we could estimate that the average size of the structures detected in Fig. 4 top was 215 µm, while the average pitch was 1350 µm; while for the structures detected in Fig. 4 bottom the size was 240 µm, while the average pitch was 1125 µm.

IV. Conclusion

In this paper we validated, by experimental tests, the theoretical framework presented in [26]. For this purpose, we designed a homemade phantom, which consisted of parallel nylon wires. Different sets of wires were built with wires having different diameters and pitches to mimic cardiac fibers. Experiments confirmed the simulation results: the SC characteristics depend on fiber orientation, P and S. As foreseen by the theory, the main-to-secondary lobe distance linearly correlated with P, while a direct relationship between the value of the SC at lag 1 and S was shown. Preliminary *in vivo* tests were also conducted on the biceps of a healthy volunteer that allowed us to estimate, from the related SC maps, average size and pitch of the structures under exams.

In conclusion, the proposed analysis of SC maps allows assessing orientation, size and pitch of fibrous structures, thereby providing additional microstructural information of the tissue under exam.

Acknowledgment

This work was performed within the framework of the LABEX PRIMES (ANR-11-LABX-0063) of Université de Lyon, within the program "Investissements d'Avenir" (ANR-11-IDEX-0007) operated by the French National Research Agency (ANR). The RF Verasonics generator was cofounded by the FEDER program, Saint-Etienne Metropole (SME) and Conseil General de la Loire (CG42) within the framework of the SonoCardio-Protection Project leaded by Pr Pierre Croisille. The authors would like to thank LabTAU for their contribution in the development of the 32x32 probe prototype compatible with a driving by 1 to 4 Verasonics Vantage 256 as well as for the provision of the probe and two Vantage 256 systems.

References

[1] E. Wilkins *et al.*, 'European Cardiovascular Disease Statistics 2017', *European Heart Network*, Feb. 2017.

[2] E. J. Benjamin *et al.*, 'Heart Disease and Stroke Statistics—2018 Update: A Report From the American Heart Association', *Circulation*, vol. 137, no. 2, pp. e67–e492, Jan. 2018.

[3] A. M. Varnava, P. M. Elliott, N. Mahon, M. J. Davies, and W. J. McKenna, 'Relation between myocyte disarray and outcome in hypertrophic cardiomyopathy', *American Journal of Cardiology*, vol. 88, no. 3, pp. 275–279, Aug. 2001.

[4] D. H. MacIver and A. L. Clark, 'Contractile Dysfunction in Sarcomeric Hypertrophic Cardiomyopathy', *J. Card. Fail.*, vol. 22, no. 9, pp. 731–737, Sep. 2016.

[5] A. J. Marian and E. Braunwald, 'Hypertrophic Cardiomyopathy: Genetics, Pathogenesis, Clinical Manifestations, Diagnosis, and Therapy', *Circulation Research*, vol. 121, no. 7, pp. 749–770, Sep. 2017.

[6] R. H. Anderson, S. Y. Ho, K. Redmann, D. Sanchez-Quintana, and P. P. Lunkenheimer, 'The anatomical arrangement of the myocardial cells making up the ventricular mass', *Eur J Cardiothorac Surg*, vol. 28, no. 4, pp. 517–

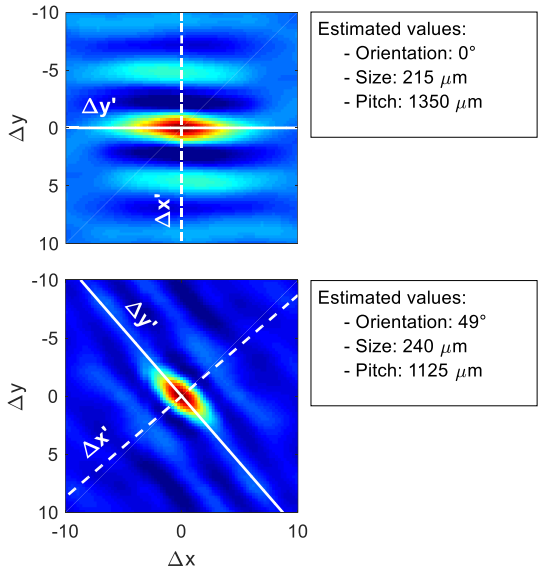

Fig. 4 Examples of in-vivo SC maps and estimated values on biceps of healthy volunteers.

525, Oct. 2005.

[7] M. J. Kocica, A. F. Corno, V. Lackovic, and V. I. Kanjuh, 'The Helical Ventricular Myocardial Band of Torrent-Guasp', *Seminars in Thoracic and Cardiovascular Surgery: Pediatric Cardiac Surgery Annual*, vol. 10, no. 1, pp. 52–60, Jan. 2007.

[8] P. P. Sengupta *et al.*, 'Left Ventricular Form and Function Revisited: Applied Translational Science to Cardiovascular Ultrasound Imaging', *Journal of the American Society of Echocardiography*, vol. 20, no. 5, pp. 539–551, May 2007.

[9] S. Y. Ho, 'Anatomy and myoarchitecture of the left ventricular wall in normal and in disease', *Eur J Echocardiogr*, vol. 10, no. 8, pp. iii3-7, Dec. 2009.

[10] T. Arts, K. D. Costa, J. W. Covell, and A. D. McCulloch, 'Relating myocardial laminar architecture to shear strain and muscle fiber orientation', *American Journal of Physiology-Heart and Circulatory Physiology*, vol. 280, no. 5, pp. H2222–H2229, May 2001.

[11] A. G. Kléber and Y. Rudy, 'Basic Mechanisms of Cardiac Impulse Propagation and Associated Arrhythmias', *Physiological Reviews*, vol. 84, no. 2, pp. 431–488, Apr. 2004.

[12] D. A. Hooks, M. L. Trew, B. J. Caldwell, G. B. Sands, I. J. LeGrice, and B. H. Smaill, 'Laminar Arrangement of Ventricular Myocytes Influences Electrical Behavior of the Heart', *Circulation Research*, vol. 101, no. 10, pp. e103–e112, Nov. 2007.

[13] F. P. Mall, 'On the muscular architecture of the ventricles of the human heart', *Am. J. Anat.*, vol. 11, no. 3, pp. 211–266, Mar. 1911.

[14] A. Keith, 'Harveian Lecture on the functional anatomy of the heart', *Br Med J*, vol. 1, no. 2987, pp. 361–363, Mar. 1918.

[15] P. F. Ferreira *et al.*, 'In vivo cardiovascular magnetic resonance diffusion tensor imaging shows evidence of abnormal myocardial laminar orientations and mobility in hypertrophic cardiomyopathy', *Journal of Cardiovascular Magnetic Resonance*, vol. 16, p. 87, Nov. 2014.

[16] A. Nagler, C. Bertoglio, C. T. Stoeck, S. Kozerke, and W. A. Wall, 'Maximum likelihood estimation of cardiac fiber bundle orientation from arbitrarily spaced diffusion weighted images', *Med Image Anal*, vol. 39, pp. 56–77, Jul. 2017.

[17] N. S. Jeffery, R. S. Stephenson, J. A. Gallagher, J. C. Jarvis, and P. G. Cox, 'Micro-computed tomography with iodine staining resolves the arrangement of muscle fibres', *Journal of Biomechanics*, vol. 44, no. 1, pp. 189–192, Jan. 2011.

[18] F. Varray, I. Mirea, M. Langer, F. Peyrin, L. Fanton, and I. E. Magnin, 'Extraction of the 3D local orientation of myocytes in human cardiac tissue using X-ray phase-contrast micro-tomography and multi-scale analysis', *Medical Image Analysis*, vol. 38, pp. 117–132, May 2017.

[19] C. P. Fleming, C. M. Ripplinger, B. Webb, I. R. Efimov, and A. M. Rollins, 'Quantification of cardiac fiber orientation using optical coherence tomography', *J Biomed Opt*, vol. 13, no. 3, p. 030505, 2008.

[20] C. Fan and G. Yao, 'Imaging myocardial fiber orientation using polarization sensitive optical coherence tomography', *Biomed Opt Express*, vol. 4, no. 3, pp. 460–465, Mar. 2013.

[21] P.-S. Jouk *et al.*, 'Analysis of the fiber architecture of the heart by quantitative polarized light microscopy. Accuracy, limitations and contribution to the study of the fiber architecture of the ventricles during fetal and neonatal life', *Eur J Cardiothorac Surg*, vol. 31, no. 5, pp. 915–921, May 2007.

[22] H. Huang *et al.*, 'Three-dimensional cardiac architecture determined by two-photon microtomy', *J Biomed Opt*, vol. 14, no. 4, p. 044029, 2009.

[23] S. A. Wickline, E. D. Verdonk, and J. G. Miller, 'Three-dimensional characterization of human ventricular myofiber architecture by ultrasonic backscatter.', *J Clin Invest*, vol. 88, no. 2, pp. 438–446, Aug. 1991.

[24] W. N. Lee *et al.*, 'Mapping Myocardial Fiber Orientation Using Echocardiography-Based Shear Wave Imaging', *IEEE Transactions on Medical Imaging*, vol. 31, no. 3, pp. 554–562, Mar. 2012.

[25] C. Papadacci *et al.*, 'Imaging the dynamics of cardiac fiber orientation in vivo using 3D Ultrasound Backscatter Tensor Imaging', *Scientific Reports*, vol. 7, no. 1, p. 830, Apr. 2017.

[26] A. Ramalli, P. Santos, and J. D'hooge, 'Ultrasound Imaging of Cardiac Fiber Orientation: What are We Looking at?', in *2018 IEEE International Ultrasonics Symposium (IUS)*, 2018, pp. 1–6.

[27] L. Petrusca *et al.*, 'Fast Volumetric Ultrasound B-Mode and Doppler Imaging with a New High-Channels Density Platform for Advanced 4D Cardiac Imaging/Therapy', *Applied Sciences*, vol. 8, no. 2, Feb. 2018.